Injection-induced Microearthquakes for Reservoir Characterization in Darajat Geothermal Field, Indonesia

Chris Nelson, Gregg Nordquist, Reka Tanuwidjaja[1] and Andrew Jupe[2]

Star Energy Geothermal Darajat[1], Altcom Limited[2]

Keywords

Microseismic, MEQ, Tomography, Velocity Model, Darajat

ABSTRACT

Since 2006, Star Energy Geothermal has continuously monitored microearthquakes (MEQs) associated with production and injection activities in the Darajat field. The 10- to 13-station array has located more than 6,800 events during this period. Experience has shown that most of the induced seismicity is related to the injection of power plant condensate and during the drilling of production make-up wells. The MEQ events around the injectors and the make-up wells are mostly observed at depths extending below the TD of the wells indicating stimulation of the deeper connected fracture system of the reservoir. These MEQ events are interpreted to be induced by thermal contraction and transient pressure increase that occur along the movement paths of the injected condensate. Traditionally, these injection-induced MEQs have been used to interpret flow directions in the reservoir for the injectate and used as "sounding" points for the interpretation of the depth extent of the connected fracture system (i.e., Base of Reservoir or BoR). For these interpretations, the locations of the MEQ's were calculated using a 1D velocity model (HYPOPLUS).

A recent velocity model improvement was conducted by developing 1D and 3D models from tomography inversion. The new velocity model reduced the overall location uncertainties and showed a distinct velocity signature in the reservoir. MEQ events located with the new 3D tomographic velocity model tend to be shallower and more tightly grouped compared to the previous model. Additionally, lower P-wave velocity (Vp) and P- and S-wave ratio (Vp/Vs) are centered over the main production area. The lower Vp extends into the area where productive entries are found in the reservoir, and may be related to the nature of the fracture system in the reservoir and phase changes in the reservoir's fractures and matrix. An attempt to model the 4D Vp/Vs changes and distribution was performed to observe phase changes after a key injection move from central to the northeast corner of the field. Interim results show a systematic small increase in the Vp/Vs ratio that extends southwest from the new injector towards the production area. Further study is underway to confirm the robustness of the inverted results.

1. Introduction

The Darajat Field is a vapor-dominated geothermal system located in West Java, Indonesia, about 150 km southeast of Jakarta (Figure 1). The field is currently operating with total installed capacity of 271 MWe from three power plants units. It is believed that the Darajat geothermal system is associated with the Kendang volcanic complex and the reservoir is composed of propylitically-altered andesite lava flows intruded by microdiorite dikes (Rejeki et al. 2010). The dominant geologic structures at Darajat trend NE-SW and NW-SE with minor N-S faults.

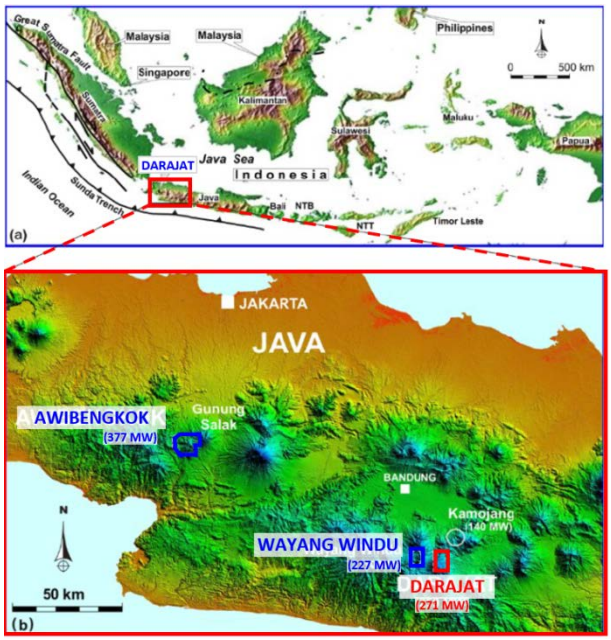

Figure 1: Location map of the Darajat geothermal field in relation with other Star Energy geothermal operations in Awibengkok (Salak) and Wayang Windu fields.

Continuous microseismic (MEQ) monitoring in Darajat has been carried out since 2006 using a network that ranged from 10 to 13 digital 24-bit recorders (SMART24 of Geotech Ltd.) distributed around the production-injection area. The sensors are three-component 4.5 hz seismometers which are buried about 1 meter below the surface. Data are uploaded weekly from the field instruments, time-associated and run through an auto picker. These MEQ events are individually checked and the P- and S-wave arrival times for the local events are handpicked. For the initial interpretation and analysis, the events are located using a 1D model (HYPOPLUS).

2. Injection-Related Seismicity

The majority of the MEQs observed at Darajat are found to be related to injection activities into the reservoir. These injection activities include routine injection of power plant condensate into designated injection wells and during production make-up well drilling. The association of

MEQs with injection of the condensate is interpreted based on the temporal correlation between the MEQ occurrence with injection, and also the spatial clustering of most MEQs near injection and make-up wells. As for injection-related seismicity at The Geysers USA, the primary induction mechanism is interpreted to be the result of relatively cool condensate (40°C) moving through the reservoir's fracture system which cools the rocks resulting in contraction, thereby, lessening the frictional forces across the fracture and allowing failure to take place (Mossop 1998; Stark 2003). During the seismic monitoring period at Darajat Field, the primary condensate injectors have been DRJ-15 (2001 to 2011) in the center of the production area and DRJ-19 (2012 to present) near the northeast field margin. Injection was also conducted in several other wells with the main ones being DRJ-3 and DRJ-12 (Figure 2).

Injection into DRJ-15 resulted into clustering of induced seismicity around and extending southwest of the well (Figure 2). MEQs correlated with the injection at DRJ-15 were concentrated parallel with the NW-SE trending Gagak Fault with the majority on the northwestern flank of the fault. The majority of the hypocenters extends well below the TD of DRJ-15 indicating the movement of the injectate to the deeper parts of the reservoir (Figure 3). A similar behavior is observed with injection-induced MEQs related to the injection in DRJ-12. The MEQ epicenters are parallel to the NE-SW Cibeureum Fault with majority of the hypocenters deeper than the well's TD. The deeply extending hypocenters and the trends of epicenters are an indication of where the fracture system is being stimulated by the movement of the condensate. The MEQs occur where the fracture system is critically stressed and connected to the commercial reservoir but of relatively lower permeability. This contrasts with the behavior of the MEQs during the injection at DRJ-3 where there is no clearly developed clustering near the well. This is most likely due to relatively low injection rates into the well and the shallow completion of the DRJ-3 into the high permeability reservoir.

By late 2011 all the condensate was injected to DRJ-19, a deep injector near northeast reservoir margin (Figure 2). The transfer of condensate injection from infield to edgefield strongly impacted the MEQ distribution at Darajat. While the central MEQ cluster is still observed, a new MEQ cluster was identified near DRJ-19. The new MEQ cluster occur deep (Figure 9) and extends west and south of DRJ-19 (Figure 4). The MEQ pattern indicated that some injectate moved deep into the reservoir until the Kendang Fault and stopped, suggesting that this structure is a permeability control of the geothermal system in northwest Darajat (Perdana 2014).

The obvious clustering of MEQs was also recognized during the drilling of make-up wells in Darajat. It has been observed that the seismicity around most of the new wells increased as soon as blind drilling with condensate started. During blind drilling in the reservoir section, power plant condensate is used instead of the denser drilling mud. The use of condensate starts after the first loss of mud circulation in the production section of the well to limit damage to the permeability of the reservoir rocks.

For the make-up wells, the largest number of MEQs were induced during the drilling of the wells near the western margin of the field (i.e., DRJ-42 and DRJ-43) (Figure 5). It is interpreted that the large number of MEQs resulted from the stimulation of existing fractures as the condensate moves through the relatively lower permeability margin of the reservoir. The distribution of MEQs during blind drilling provides seismicity information in the area outside of regular injection activities. MEQs commonly located along similar trends with the nearest fault suggests

that the condensate is moving along or parallel to fracture networks related to these structures (Irfan 2013).

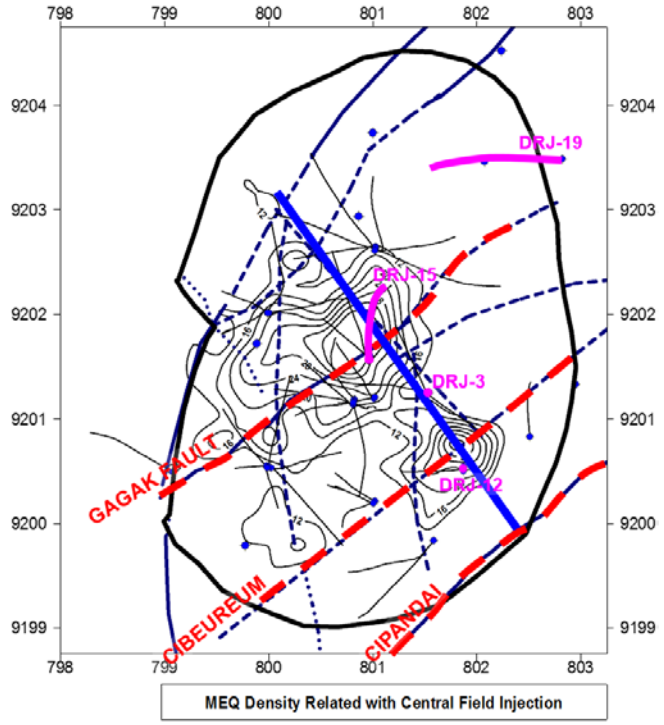

Figure 2: MEQ density map (black contour) showing the areas influenced by the injection at DRJ-15 and DRJ-12 (but excluding the MEQs from the drilling and later injection into DRJ-19). The NW-SE profile line of the cross section in Figure 3 is also shown as the blue line.

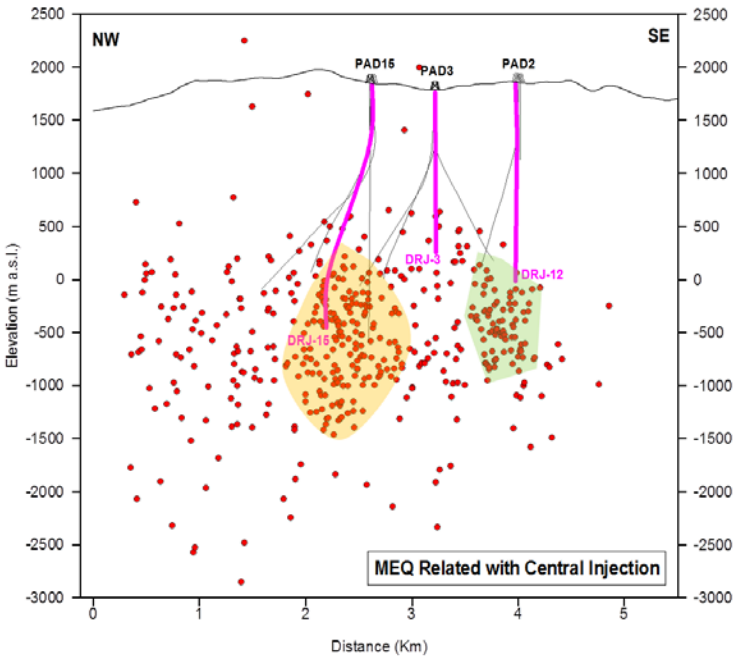

Figure 3: Cross-section showing the distribution of injection-induced MEQ hypocenters around DRJ-15 and DRJ-12. Most of the events are located below the wells' TD. Profile line is shown in Figure 2.

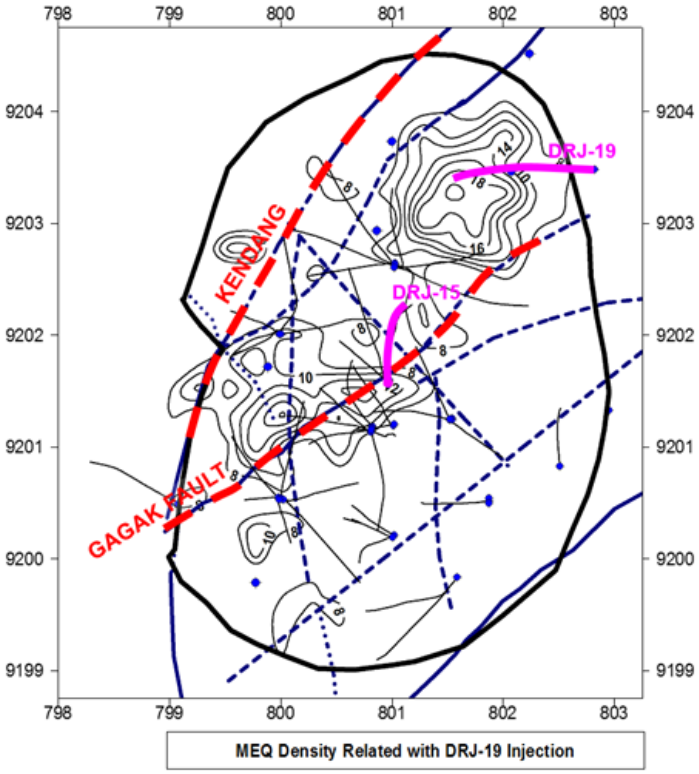

Figure 4: MEQ density map (black contour) showing the area influenced by injection into DRJ-19. Kendang and Gagak geological structures are highlighted by red dashed line.

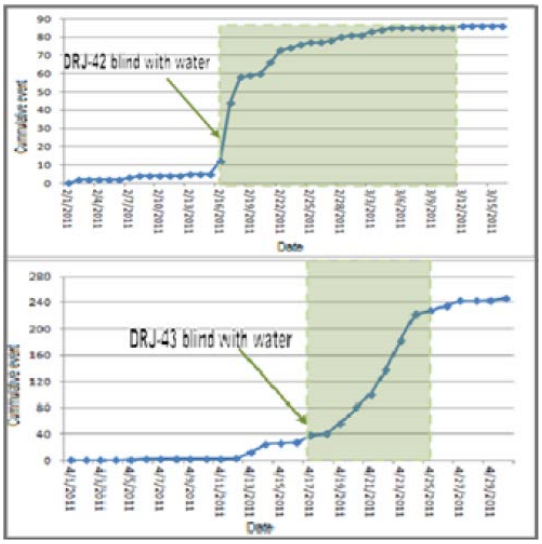

Figure 5: Temporal correlation showing the period of blind drilling and seismicity rates near DRJ-42 and DRJ-43 (Irfan 2013)

3. Utilizing MEQ for Reservoir Characterization

An important priority for Star Energy Geothermal (SEG) is to leverage the extensive database of local MEQ events (>6,800) for reservoir characterization. The MEQ data provide a dataset of hypocenters and epicenters that appear to delineate the reservoir fracture system.

The subject of this paper is a description of the workflows used during the updating of the 1D velocity model and developing a 3D tomography model (Vp and Vs). Also described are the preliminary results and conclusions from these new velocity models. Other activities currently underway include testing of the Double Difference approach (Waldhauser and Ellsworth 2000) and determination of focal mechanisms in an attempt to better image the reservoir fracture system and to understand the fracture mechanism. Also, SEG is looking at the application of S-wave splitting for quantification of fracture anisotropy and density (e.g. Lou and Rial 1997). The scope of this paper is, however, limited to the new velocity modeling and its results and interpretations. The other studies will be topics for future papers.

For the new velocity modeling, SEG has been working with Altcom Ltd. and utilizing their Microseisgram software and a recently added tomographic modeling module - JTOMO. At the time when the most recent tomography run was performed, about 6,488 MEQ events have been catalogued in the Microseisgram database within the period which provided 41,096 P-wave and 38,379 S-wave arrival times. This tomography study utilized a filtered subset of the data resulting in utilization of approximately 45% of the data set. The filtering was selected based on the minimum number of station (≥5), maximum error ellipsoid (≤300 m), and maximum residual time (≤0.25 s).

JTOMO provides a flexible framework for building complex inversion workflows consisting of the following components:

- P- and S-wave 1D or 3D velocity tomography
- Event location
- Station delay terms
- Double-Difference event location

The inversion solution is based on the LSQR method by Paige and Saunders (1982) and each component can be inverted independently, sequentially or simultaneously. Therefore, a simultaneous location and station-delay inversion is equivalent to a Joint Hypocenter Determination (JHD) (Douglas 1967), and the inclusion of all components is equivalent to the Double-Difference Tomography method (Zhang and Thurber 2003). In this study, SEG generally used sequential location, 1D/3D velocity, and station-delay inversions.

Typically, seismicity inversion also tends to focus on a relatively small, highest quality, subset of the events. However, an important objective in this study has been to build robust inversion workflows that incorporate the majority of the available data. This is achieved with JTOMO through the ability to interact closely with the inversion process, rapidly plot and diagnose behavior, and easily adjust and optimize the workflow. JTOMO has also been applied to data sets from hydraulic fracturing in shale, conventional hydrocarbon production, and Engineered Geothermal Systems (EGS) where data sets range in size from a few hundred to tens of thousands of MEQ events.

4. Velocity Tomography Workflow

For velocity modeling, new workflows were developed for 1D and 3D tomography. The workflow for the tomography run is summarized in Figure 6. The overall strategy was to first solve for the best 1D (horizontally-layered) model using the initial MEQ locations and a half-space starting model, then secondly continue with a joint 3D inversion using the 1D model result as the new starting model. The overall final model was obtained after several 3D inversions which resulted in a stable and consistent velocity structures.

Therefore, the velocity model determination begins with a 1D inversion using a half-space starting model and initial locations derived from the original 1D model (Geosystem 2003). Both P- and S-wave first-arrival times were simultaneously inverted for earthquake location and 1D Vp and Vs velocity model parameters. The results from the first inversion was utilized as the starting velocity for the following inversions and so on. Once the preceding inversion indicates a stable result, the 1D model is finalized.

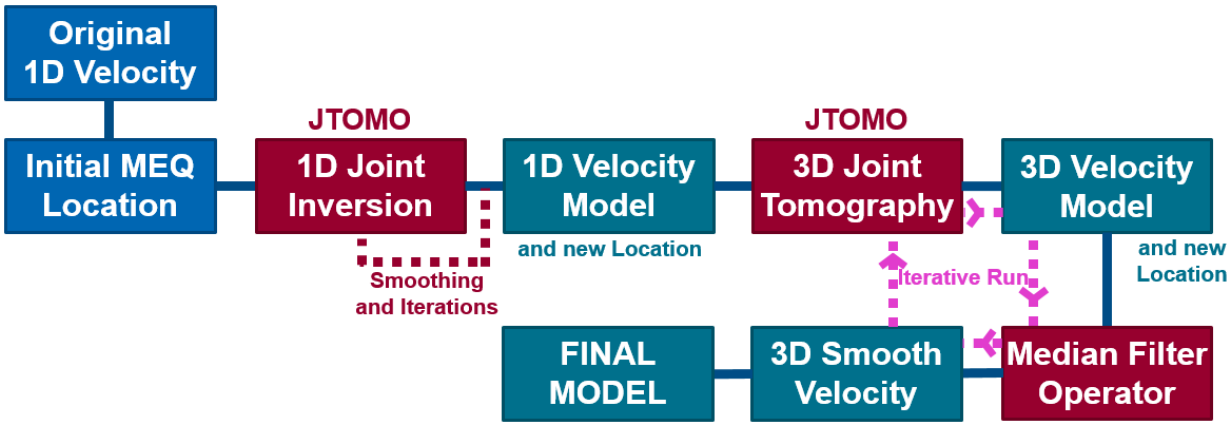

Figure 6: Diagram showing 1D & 3D velocity tomography workflow applied in this study.

The final 1D Vp velocity model and its layered structures are shown in Figure 7. This new velocity model is similar to the original model in the shallow layers but diverges at greater depths. Another important result was the Vs velocity model. This new Vs model results in an average Vp/Vs ratio of 1.72, compared to a Vp/Vs estimate of 1.66 used in the original model (which was based on a limited data set and used the Wadati method). New MEQ locations were then generated using this updated 1D velocity model and kept as starting location for the 3D inversion.

The starting model for the first pass 3D tomography inversion was the revised 1D model (Figure 7). The model space was gridded with 250-meter grid blocks. Station delay calculation was incorporated to solve near-surface velocity uncertainties and station location effects. In addition, the fraction of the calculated velocity grid perturbation that was applied during subsequent iterations was adjusted to provide more stability and control over how the model converged. A typical number of iterations was 100.

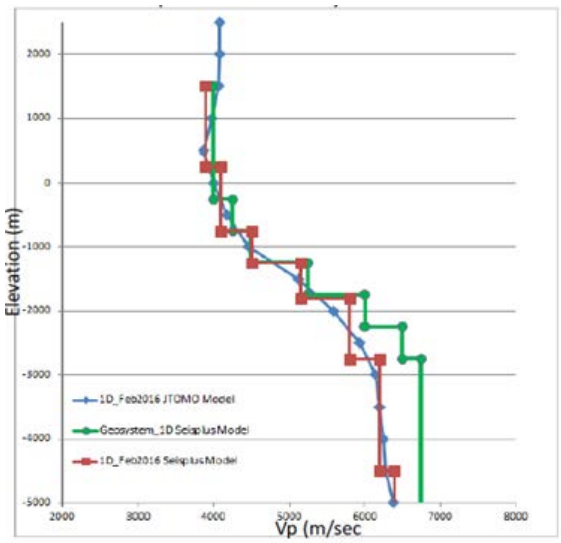

Figure 7: Chart showing the smoothed Vp model from the 1D JTOMO inversion (blue) and the corresponding stair step model (red). A comparison to original 2003 model (green) is also shown (Nordquist 2016).

This step resulted in the first pass 3D tomography velocity model. This model was loaded into the 3D static modeling software GoCAD and smoothed using a median-smoothing operation, which smooths through the occasional velocity "bullseyes" and results in a smoother velocity model. This is done for both the Vp and Vs models. These new models are then used as initial guesses for the subsequent tomography run. The process is repeated until a consistent and stable velocity can be reached. A W-E profile across the field shows an example of stable velocity after three sequential runs (Figure 8).

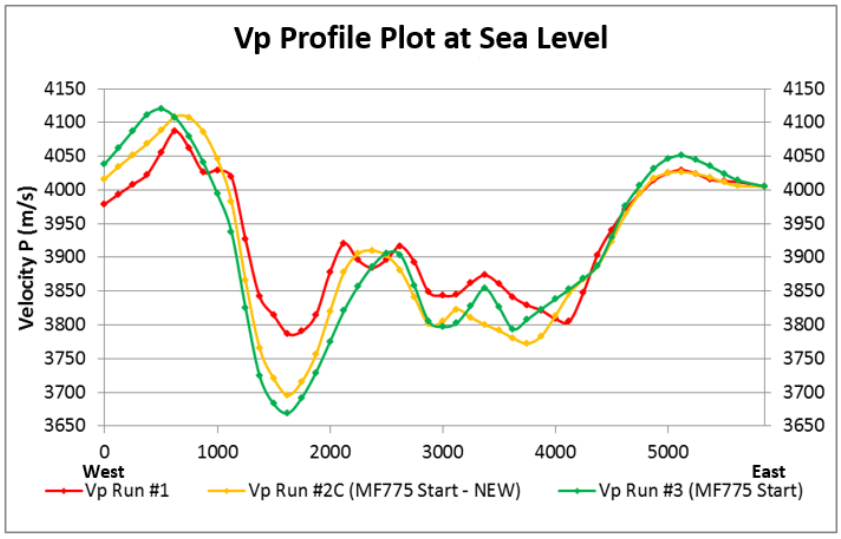

Figure 8: Profile plot showing the evolution of Vp velocity from 1st-2nd-3rd tomography runs. The profile line is shown in Figure 11.

5. Results and Discussion

The resulting 3D tomography model provides an image of the velocity structure through the inverted microseismic events between 2007 and 2016. Key uncertainty indicators such as P- and S-phases residual mean (observed vs calculated arrival times) and error ellipsoid distribution showed distinct improvements for the final 3D velocity model compared to the original 1D model. The new residual mean distribution indicates tighter and a more-centered distribution near zero difference. Meanwhile, the maximum error ellipsoid distributions are now shifting to the left of the previous curves which indicates reduction on location uncertainty.

In general, MEQ events located with the new velocity model result in a shift of the epicenters to the east-northeast direction with shallower depth compared to their previous locations. Figure 9 shows an example along a N-S line that includes clusters from the DRJ-15 and DRJ-19 condensate injectors. There has been a marked tightening of the clusters of MEQs as well as some shallowing of the base of the clusters. This is most evident near DRJ-19 and the southern portion of the Darajat Field. These updated hypocenter locations have been utilized to map the depth extent of the connected fracture system. MEQ event densities are computed in the static earth model and gridded to determine the BoR. As shown in Figure 10, the new base of the connected fracture network surface is interpreted to be shallower in the southern portion of the Darajat Field, with only a slight change in central and northern portions.

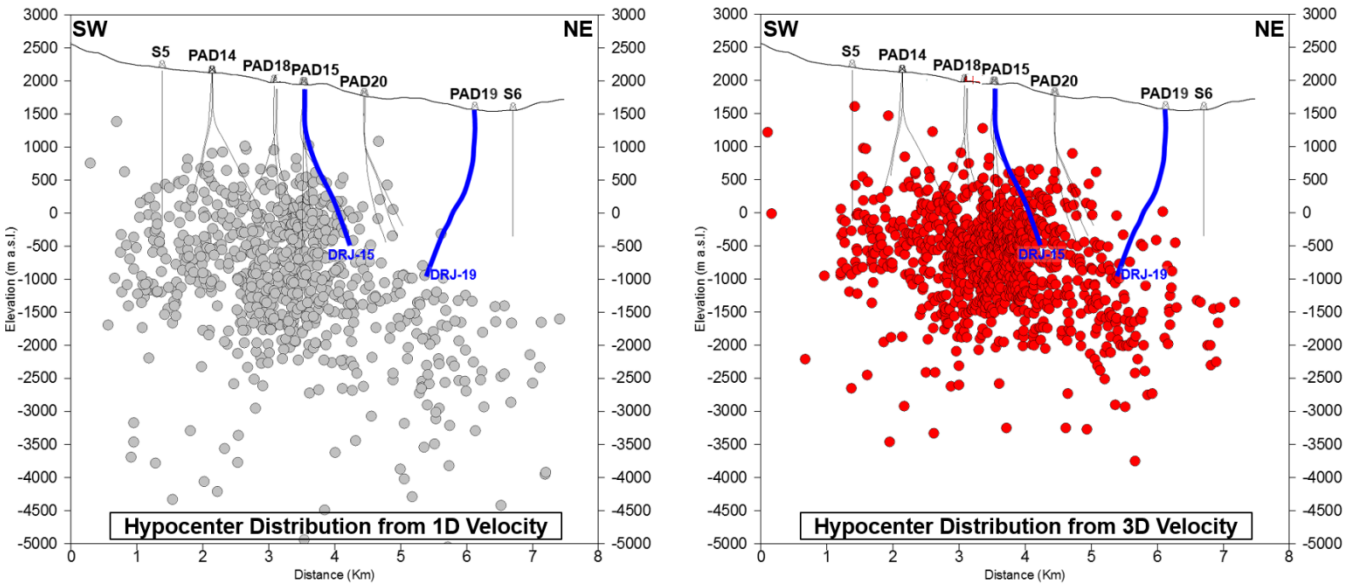

Figure 9: SW-NE cross-sections showing the distribution of the hypocenters from original 1D velocity model (left, grey circles) and hypocenters from final 3D model (right, red circles). In general, MEQ event locations are more tightly grouped and shifted to shallower depth.

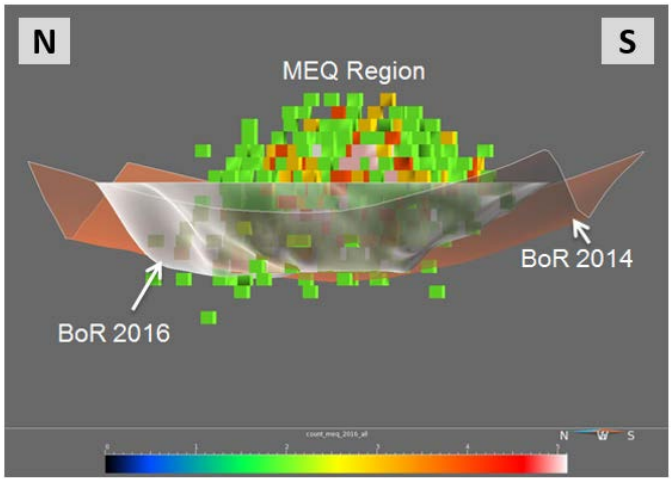

Figure 10: Cross-section showing the evolution of the BoR (or the base of the connected fracture network) from the 2014 (orange surface) to the tomography-influenced 2016 model (white surface). MEQ distributions are marked by the colored cubes. Denser events are indicated by warmer cell block.

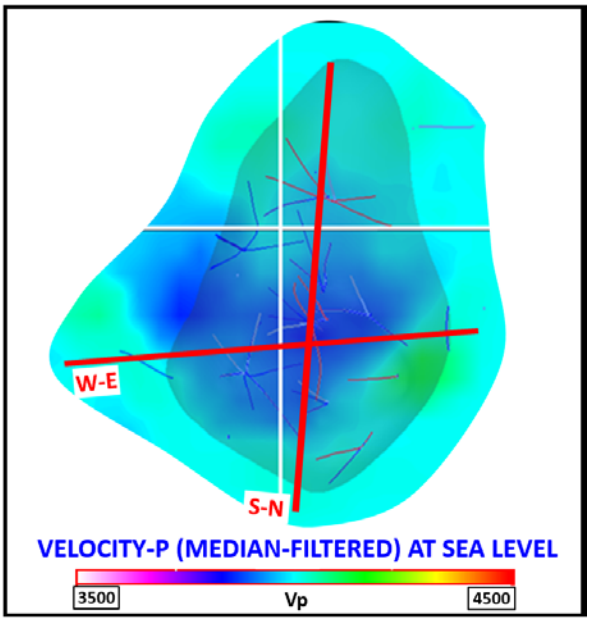

Figure 11: Map showing the distribution of Vp velocity model at Mean Sea Level (MSL). Colder color shading indicates the lower P-wave velocity. Also shown, the W-E and N-S profile lines (red) refer to Figures 8 and 15.

The imaged velocity structure from the 3D tomographic model delineates a distinct variation of velocity signatures within the Darajat reservoir. Relatively lower Vp velocity are shown in the central and southern portions of the field. In contrast, slightly higher velocities are observed in the southeastern and northern-most parts of the reservoir (Figure 11). This pattern of velocity structure is further highlighted with the distribution of Vp/Vs ratio (Figure 12) with a distinctly lower Vp/Vs located over the central portion of the field. The central and southern areas are where steam production has been occurring for more than two decades at Darajat. These regions

have experienced the highest reservoir pressure drop (Figure 13) and steam saturation increases in the reservoir matrix which correspond to the low Vp/Vs bowl in Central Darajat. Thus, the relatively lower Vp and Vp/Vs ratio is interpreted to result from a decrease in the compressional velocity (Vp) due in part at least to changes related to the mass extraction in the field.

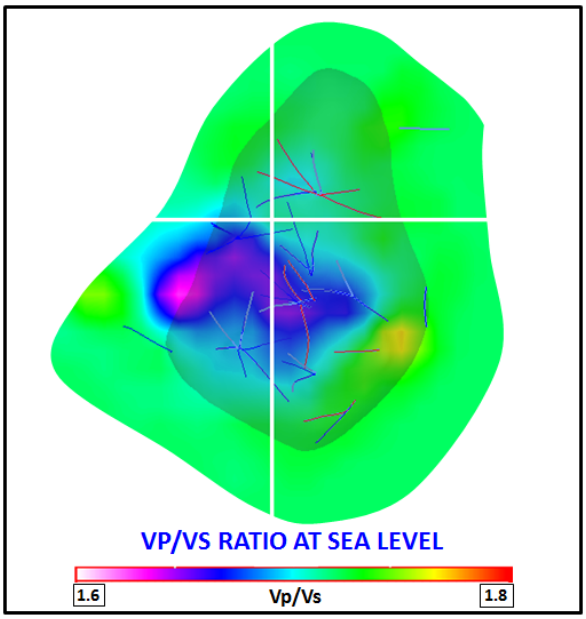

Figure 12: Map showing the distribution of Vp/Vs ratio at Mean Sea Level (MSL). Colder color shading in central Darajat indicates the lower P-wave and S-wave velocity ratio.

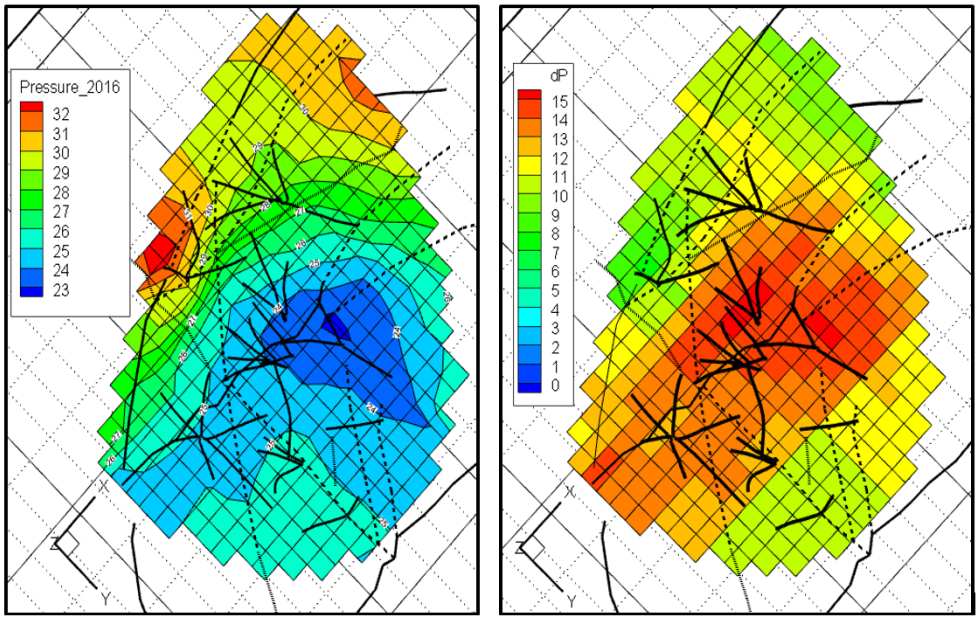

Figure 13: Map showing the distribution of reservoir pressure in 2016 (left) which indicates the lowest pressure area on the central production of Darajat Field (blue color). Also shown, the Δ-pressure between the pre-exploitation state of the reservoir and the 2016 (right). The biggest Δ-pressure is shown by the warmer color cell block.

This conclusion is supported by the link between Vp/Vs and the modeled steam saturation in the matrix through 2016 using the Darajat numerical simulator (Figure 14-A). Although the coefficient of determination (R^2) of the cross-plot still indicates variability of the response data, the observable trend shows an inverse correlation between Vp/Vs and matrix steam saturation. Similar trends of lower Vp and Vp/Vs ratios have also observed in other steam-dominated geothermal field such as The Geysers, USA and Larderello, Italy (Gunasekera et al. 2003; De Matteis et al. 2010).

A cross-plot between modeled matrix pressure and Vp also indicates a relationship of lower Vp as pressure decreases in the matrix (Figure 14-B). This is uncharacteristic as a decrease in pressure generally results in increased Vp (Gunasekera et al. 2002). This apparent correlation may be mostly driven by the increased steam saturation in the matrix as the pressure decreases.

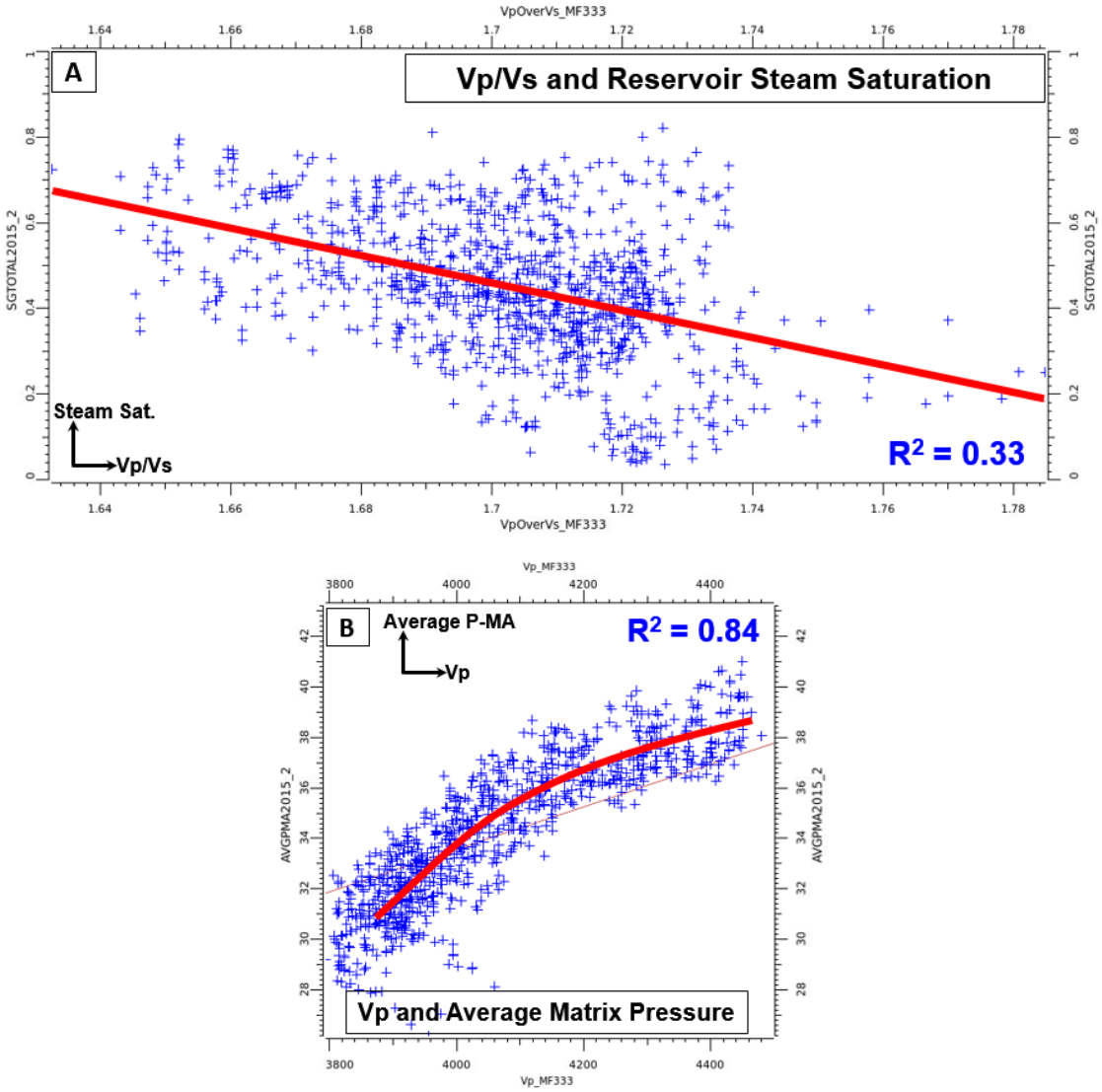

Figure 14: Scatter plots showing the correlation between modeled steam saturation and pressure in the matrix, i.e., (A) Vp/Vs ratio and reservoir steam saturation and (B) Vp velocity and average matrix pressure.

A N-S profile through the field shows the variation of Vp velocity at sea level (Figure 15). The profile highlights the distinct area with lower Vp south of the Gagak Fault, where production has been taking place since 1994. Significant production north of the fault started in 2007 with the commissioning of the power plant Unit III. Both main injectors DRJ-15 (2000 – 2011) and DRJ-19 (2012 to present) are located north of the fault. Combining the role of Gagak Fault in the velocity model and the distribution of MEQ events during injection at DRJ-15 and DRJ-19 (Figures 2 and 4) indicates that this structure is acting as a compartment divider and, possibly, a semi-barrier within the reservoir, likely playing an important role in the channeling of the condensate injectate.

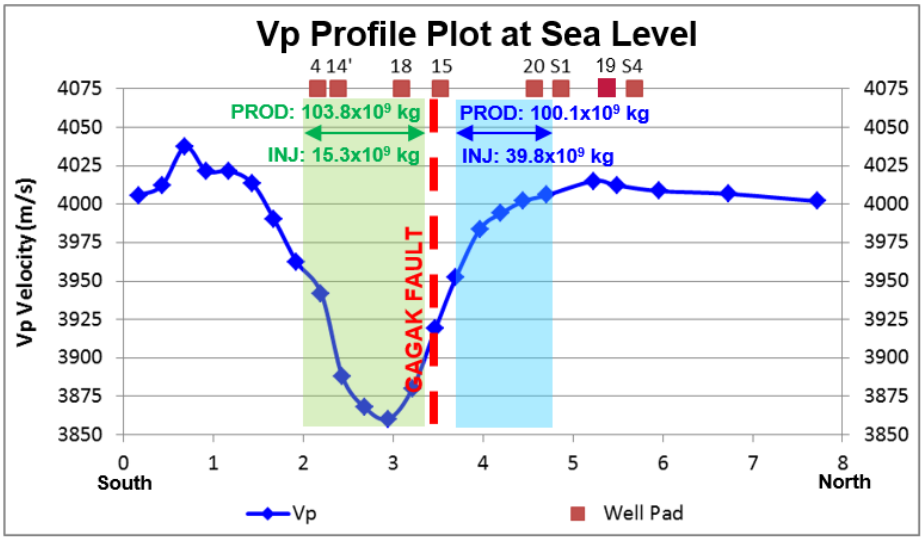

Figure 15: Profile showing the trend of Vp velocity from South to North Darajat at MSL. Vp is noticeably higher at the northern side of the Gagak Fault. The profile line is shown in Figure 11.

To understand the dynamic velocity evolution throughout the microseismic monitoring period, a time-lapse (4D) velocity tomography modeling was performed in two separate time intervals. The microseismic data was broken into shorter time periods, namely, 2006 to 2011 and 2012 to 2016. The first time period corresponds to infield injection at DRJ-15 in Central Darajat while the second period refers to edgefield injection at DRJ-19 in northeast Darajat.

For the interpretation of 4D changes in the reservoir, the most common parameter used is the Vp/Vs ratio. Low Vp/Vs ratio is dominant in the central portion of the field during both time intervals (Figure 16). This trend is similar to the general velocity pattern described earlier. A notable variation, however, can be clearly seen in the northeast region where Vp/Vs distribution in 2011-2016 is higher which corresponds spatially with the location of DRJ-19.

The difference in velocity variation between the two time intervals can be examined by highlighting the change of Vp/Vs ratio between both periods. Figure 17 shows the distribution of positive change (in %) near DRJ-19 during the second time period. Although the overall difference is relatively small (<2% change), this positive pattern appears to be systematic

showing an increased Vp/Vs which trends southwest away from DRJ-19. An increased ratio is consistent with what would be expected for increased fluid saturation in the fractures and, possibly, rock matrix. A separate study from 4D microgravity monitoring supports this interpretation by exhibiting near zero gravity change in the northern portion of the field due to the effect of injection at DRJ-19 (Nelson, 2016).

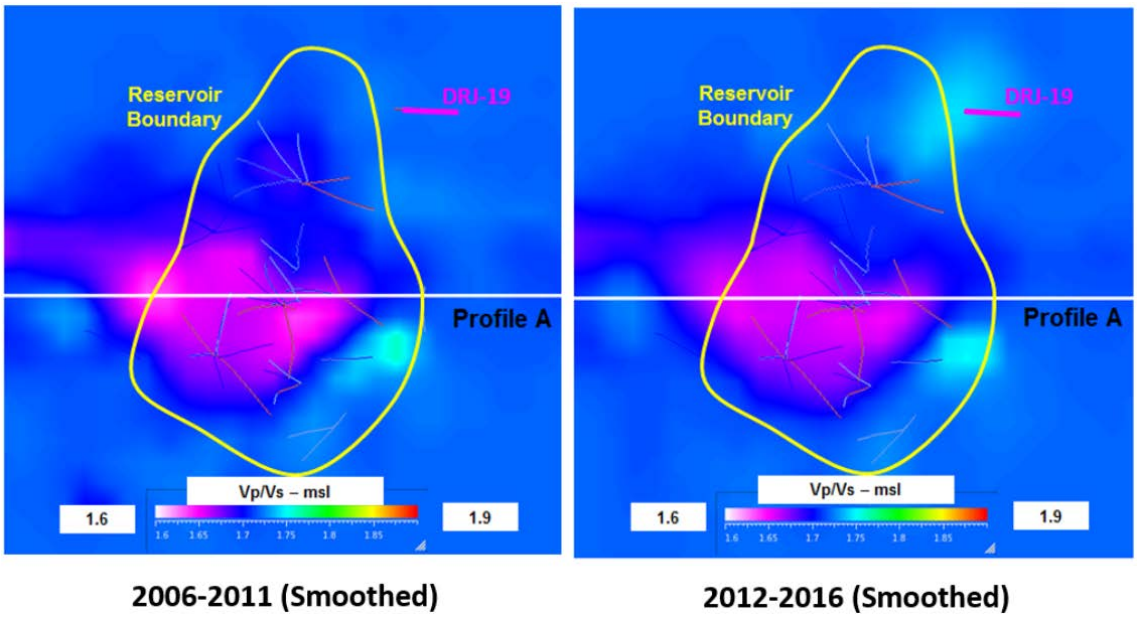

Figure 16. Maps showing lateral Vp/Vs distribution at MSL during 2006-2011 (left figure) and 2012-2016 period (right figure). The colder color shading indicates the lower Vp/Vs velocity ratio in Central Darajat.

The positive Vp/Vs pattern parallels the Gagak Fault and extends away from DRJ-19 towards the Pad-20 region. The systematic SW-NE trend has a similar alignment to the maximum horizontal stress direction of the field that indicates the dominant SW-NE direction of the fracture system orientation in Darajat. In addition, the positive velocity changes in the northern side of Gagak Fault supports the consistent role of the structure as a compartment divider in Darajat.

6. Conclusions

The implementation of new techniques of microseismic processing and tomography incorporated in the Microseisgram/JTOMO software has provided important new insights on the understanding of the fracture network and reservoir management at Darajat Field. Recent velocity models have reduced the overall uncertainty of the MEQ hypocenters and have improved velocity images of the field. The distribution of Vp and Vp/Vs variations from the tomography model has been correlated to major field operations (i.e., production and infield and edgefield injection) and reservoir features at Darajat (i.e., reservoir thermodynamics properties, fractures orientation, and fault compartmentalization). Continuous effort and experimentation are

being performed to improve the understanding of the conceptual meaning of the tomography results, as well as improving the technical workflow.

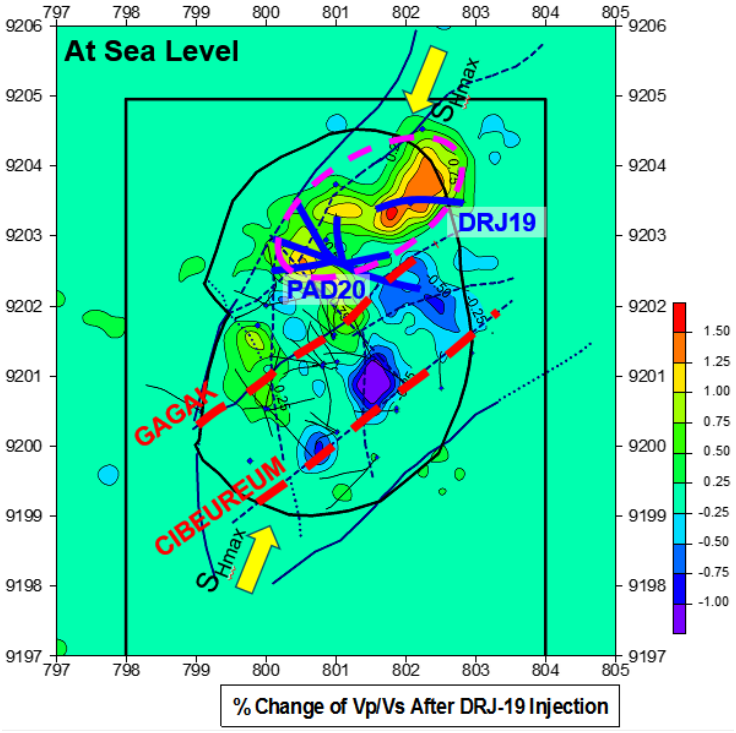

Figure 17. Maps showing Vp/Vs % change between two different time windows (2006-2011 and 2012-2016) at sea level. The warmer color shading indicates the positive % change of Vp/Vs; while in contrast, the colder color shading indicates the negative % change of velocity ratio.

Acknowledgement

The authors thank Star Energy Geothermal Darajat (SEGD) for supporting the research and improvement of the Microseisgram application, support the continuation of this project, and granting permission to publish this paper.

REFERENCES

De Matteis, R., Vanorio, T., Zollo, A., Ciuffi, S. and Fiordelisi, A. "Three-dimensional tomography and rock properties of the Larderello-Travale geothermal area, Italy." *Physics of the Earth and Planetary Interiors, Elsevier* (2010).

Douglas, A. "Joint Epicentre Determination." *Nature,* 215, (1967), p. 47–48.

Geosystem srl. "Darajat Microseismic Studies-Seismic Tomography and Moment Tensor and Analysis." *Unpublished report prepared for Amoseas* (2003).

Gunasekera, R., Foulger, G., and Julian, B. "Reservoir depletion at The Geysers geothermal area, California, shown by four-dimensional seismic tomography." *JGR*, Vol. 108, (2003), NO. B3.

Irfan, R., and Nordquist, G. "Microearthquake Monitoring During 2009-2011 Drilling Campaign Darajat Geothermal Field, Indonesia." *Proceedings: The 11th Annual Indonesian Geothermal Association Meeting & Conference* (2011).

Lou, M., and Rial J.A. "Characterization of geothermal reservoir crack patterns using shear-wave splitting." *Geophysics*, Vol. 62, (1997), p. 487–494

Mossop, A. unpublished work on mechanisms of Geysers injection-induced seismicity, (1998), *available at Stanford University c/o Dr. Paul Segall*.

Nelson, C. "Darajat Field 2016 Precision Gravity Survey – Operation Report." *Unpublished Chevron Geothermal Report* (2016).

Nelson, C., Tanuwidjaja, R., Intani, R., Pakpahan, R. "Velocity Model Determination for Reservoir Characterization in Darajat Geothermal Field." *Proceedings: The 5th Indonesia International Geothermal Convention & Exhibition* (2017).

Nordquist, G. "Darajat - Updated Velocity Model and Next Steps – First Application MicroSeisGram/ JTomo." *Unpublished Chevron Geothermal Memorandum* (2016).

Paige, C., and Saunders, M. "LSQR: sparse linear equations and least squares problems." *ACM Trans. Math. Softw*. 8, 2, (1982), p. 195–209.

Perdana, M., and Nelson, C. "Microseismic Monitoring in Darajat Geothermal Field: Observation in Moving Injection to DRJ-AI Well." *Proceedings: The 2nd Indonesia International Geothermal Convention & Exhibition* (2014).

Rejeki, S., Rohrs, D., Nordquist, G., and Fitriyanto, A. "Geologic Conceptual Model Update of the Darajat Geothermal." *Proceedings: World Geothermal Congress 2010* (2010).

Stark, M.A. "Seismic Evidence for a long-lived Enhanced Geothermal System (EGS) In the Northern Geysers Reservoir." *In Monograph on The Geysers geothermal field, Geothermal Resource Council*, Vol 27, (2003), p. 727-731.

Waldhauser, F., and Ellsworth, W. "A Double Difference Earthquake Location Algorithm: Method and Application to the Northern Hayward Fault." *California Bulletin of the Seismological Society of America*, 90, 6, (2000), p. 1351-1368.

Zhang, H., and Thurber, C. “Double-Difference Tomography: The method and its application to the Hayward Fault, California.” *Bulletin of the Seismological Society of America*, 93, 5, (2003), p. 1875-1889.